

Control of nonlinear optical phenomena and spatially structured optical effects in a four-level quantum system near a plasmonic nanostructure

Hamid Reza Hamed^{1,*}, Vassilios Yannopoulos^{2,†} and Emmanuel Paspalakis^{3,‡}

¹*Institute of Theoretical Physics and Astronomy,
Vilnius University, Saulėtekio 3, Vilnius LT-10257, Lithuania*

²*Department of Physics, National Technical University of Athens, Athens 157 80, Greece*

³*Materials Science Department, School of Natural Sciences, University of Patras, Patras 265 04, Greece*

We investigate the nonlinear optical response of a four-level double-V-type quantum system interacting with a pair of weak probe fields while located near a two-dimensional array of metal-coated dielectric nanospheres. Such a quantum system contains a V-type subsystem interacting with surface plasmons, and another V-type subsystem interacting with the free-space vacuum. A distinctive feature of the proposed setup is its sensitivity to the relative phase of the applied fields when placed near the plasmonic nanostructure. We demonstrate that due to the presence of the plasmonic nanostructure, the third-order (Kerr-type) susceptibility for one of the laser fields can be significantly modified while another probe field is acting. Moreover, the Kerr nonlinearity of the system can be controlled and even enhanced by varying the distance of the quantum system from the plasmonic nanostructure. We also show that the Kerr nonlinearity of such a system can be controlled by adjusting the relative phase of the applied fields. The results obtained may find potential applications in on-chip nanoscale photonic devices. We also study the light-matter interaction in the case where one probe field carries an optical vortex, and another probe field has no vortex. We demonstrate that due to the phase sensitivity of the closed-loop double V-type quantum system, the linear and nonlinear susceptibility of the nonvortex probe beam depends on the azimuthal angle and orbital angular momentum (OAM) of the vortex probe beam. This feature is missing in open four-level double V-type quantum system interacting with free-space vacuum, as no quantum interference occurs in this case. We use the azimuthal dependence of optical susceptibility of the quantum system to determine the regions of spatially-structured transmittance.

I. INTRODUCTION

Recently, it has been revealed that nonlinear optical effects can be significantly modified and eventually enhanced at the nanoscale when quantum systems are placed near plasmonic nanostructures. The strong modification of nonlinear effects is attributed to the large enhancement of the applied electric field, the substantial modification of the spontaneous decay rate, and the strong exciton-plasmon coupling for quantum systems near plasmonic nanostructures. Many interesting phenomena have been pointed out in this research area including gain without inversion [1–6], optical transparency and slow light [7–9], the manipulation of spontaneous emission [10–14], Fano effects in energy absorption [15–18], optical bistability [19–21], enhanced second-harmonic generation [22] and four-wave mixing [23–25].

Kerr nonlinearity, which is proportional to the third-order susceptibility, plays a crucial role in nonlinear and quantum optics. A large third-order nonlinear susceptibility [26–29] is of interest as it can be used for the realization of single-photon nonlinear devices [30, 31]. However, for many years experimental research on quantum nonlinear optics has been limited due to the weak nonlinear response of the available materials. Recently, modification, and in particular enhancement, of the Kerr nonlinearity near plasmonic nanostructures have been proposed and analyzed [32–37].

A particular quantum system with interesting optical response is the four-level double-V quantum system. When located near a two-dimensional array of metal-coated dielectric nanosphere, this scheme exhibits quantum interference in spontaneous emission [12]. Namely, it was shown that optical transparency associated with slow light [7] and the strongly modified Kerr nonlinearity [32] appear in this system when interacting with a single weak probe beam of light near the periodic plasmonic nanostructure. If the system interacts with two laser fields, an extra degree of control can be realized exploiting the extra field as well as the phase difference of the applied fields. The later gives rise to phase dependent optical effects [5, 8]. However, the control of Kerr nonlinearity for this quantum system under the interaction with two laser fields has not been yet analyzed.

* hamid.hamed@tfai.vu.lt

† vyannop@mail.ntua.gr

‡ paspalak@upatras.gr

Growing attention has recently emerged in the generation of twisted light beams due to their potential application in quantum information processing [38], optical micromanipulation [39], biosciences [40] and microtrapping and alignment [41]. Such beams of light (the so-called optical vortices) carry orbital angular momentum (OAM) with helical wavefronts focusing to rings, rather than points. The interaction of such structured light beams with cold atoms results in a plethora of interesting effects, such as light-induced-torque [42], atom vortex beams [43], entanglement of OAM states of photon pairs [44], OAM-based four-wave mixing [45, 46], spatially dependent electromagnetically induced transparency (EIT) [47–50], vortex slow light and transfer of optical vortices [51–59].

An interesting topic is the interplay of quantum systems near plasmonic nanostructures and optical vortices. The usage of the optical vortex beam together with a plasmonic nanostructure may result in a significant modification of optical response for the quantum system when compared to the case where the quantum system is just in free space. To the best of our knowledge, a similar analysis on interaction of quantum plasmonic nanostructures and structured light has not been reported.

In the present work, we explore the nonlinear optical properties of the four-level double-V-type quantum system interacting with a pair of weak probe fields and placed near a two-dimensional array of metal-coated dielectric nanospheres. The double-V-type system has two V-type subsystems. The upper V-type subsystem is influenced by its interaction with localized surface plasmons, while the other V-type subsystem interacts with the free-space vacuum. By means of a density matrix method, we calculate the linear and nonlinear optical susceptibilities for one of the laser fields in the presence of the other field and the plasmonic nanostructure. We demonstrate that the presence of the plasmonic nanostructure results in significant modification, and even enhancement, of the third-order nonlinear susceptibility for one of the probe fields. We find that the nonlinear optical susceptibility of the quantum system can be controlled through different external parameters such as the distance of the quantum system from the nanostructure as well as the relative phase between applied fields.

We also study the interaction of the double V-type system next to the periodic plasmonic nanostructure with a pair of probe laser fields, where one of the laser fields carries OAM, while the other probe laser field is a nonvortex beam. In particular, we study the angular dependence of optical susceptibility of the quantum system. We show that the azimuthally varying linear and nonlinear patterns can be controlled through different external parameters such as the distance of the quantum system from the surface of plasmonic nanostructure and the vorticity of twisted probe beam. Finally, we demonstrate that such a scheme can be used to distinguish the OAM state of a weak vortex beam by mapping the absorption of nonvortex probe field in the transverse spatial profile.

II. THEORETICAL MODEL AND FORMULATION

The quantum system under study is presented in Fig. 1(a): a four-level system containing two closely lying upper states $|2\rangle$ and $|3\rangle$, and two lower states $|0\rangle$ and $|1\rangle$, making a four-level double-V quantum system. The quantum system is in vacuum and at distance d from the surface of the plasmonic nanostructure. It is placed right opposite the center of a nanosphere, i.e., at the center of the 2D unit cell of the (periodic) plasmonic nanostructure. At this (lateral) placement of the quantum system, the resulting quantum interference p is maximized. The states $|2\rangle$ and $|3\rangle$ denote two Zeeman sublevels ($J = 1$, $M_J = \pm 1$). The two lower states $|0\rangle$ and $|1\rangle$ are corresponding levels with $J = 0$. One can define a dipole moment operator as

$$\vec{\mu} = \mu'(|2\rangle\langle 0|\hat{\epsilon}_- + |3\rangle\langle 0|\hat{\epsilon}_+) + \mu(|2\rangle\langle 1|\hat{\epsilon}_- + |3\rangle\langle 1|\hat{\epsilon}_+), \quad (1)$$

where $\hat{\epsilon}_\pm = (\mathbf{e}_z + i\mathbf{e}_x)/\sqrt{2}$ stand for the right-rotating ($\hat{\epsilon}_+$) and left-rotating ($\hat{\epsilon}_-$) unit vectors, while μ and μ' are real.

We assume that the quantum system interacts with two circularly polarized continuous-wave electromagnetic laser fields with total electric field

$$\vec{E}(t) = \hat{\epsilon}_+ E_a \cos(\omega_a t + \phi_a) + \hat{\epsilon}_- E_b \cos(\omega_b t + \phi_b), \quad (2)$$

where $E_a(E_b)$ characterizes the electric-field amplitude, $\omega_a(\omega_b)$ denotes the angular frequency, and $\phi_a(\phi_b)$ is the individual phase for the field $a(b)$. The laser field a acts between the lower level $|0\rangle$ and the upper state $|2\rangle$. The second laser field b couples the lower level $|0\rangle$ to the upper state $|3\rangle$. The transition $|0\rangle \leftrightarrow |1\rangle$ is dipole forbidden. Note that both fields are taken to have equal frequencies $\omega_a = \omega_b = \omega_L$.

Next, we assume that the upper V-type subsystem containing the states transitions $|2\rangle$, $|3\rangle$ and $|1\rangle$ lies within the surface-plasmon bands of the plasmonic nanostructure, whereas the lower V-type subsystem with states $|2\rangle$, $|3\rangle$ and $|0\rangle$ is spectrally distant from the surface-plasmon bands, and it is therefore not affected by the plasmonic nanostructure [12]. As a result, the spontaneous decay in lower V subsystem occurs because of the interaction of the quantum system with the free-space vacuum electromagnetic modes. This quantum system can be realized in hyperfine sublevels of

D lines in alkali-metal atomic systems, such as ^{85}Rb and ^{87}Rb [8, 9, 14]. Similar interactions can also be realized in quantum dots, like in dual CdSe/ZnS/CdSe quantum dots [8, 9].

The dynamics of the system is described from the master equation

$$\dot{\rho}_s = -\frac{i}{\hbar}[H_e, \rho_s] + \mathcal{L}\rho_s, \quad (3)$$

with

$$H_e = \hbar \left[\left(-\delta - \frac{\omega_{32}}{2} \right) |2\rangle\langle 2| + \left(-\delta + \frac{\omega_{32}}{2} \right) |3\rangle\langle 3| - \left(\frac{\Omega_a e^{i\phi_a}}{2} |0\rangle\langle 2| + \frac{\Omega_b e^{i\phi_b}}{2} |0\rangle\langle 3| + \text{H.c.} \right) \right], \quad (4)$$

where $\Omega_a = \mu' E_a / \sqrt{2}\hbar$ and $\Omega_b = \mu' E_b / \sqrt{2}\hbar$ are the Rabi frequencies for the two fields. The parameter $\delta = \omega_L - \tilde{\omega}$ is the detuning from resonance with the average transition energy of states $|2\rangle$ and $|3\rangle$ from state $|0\rangle$ [$\tilde{\omega} = (\omega_2 + \omega_3)/2 - \omega_0$] and $\omega_{32} = (\omega_3 - \omega_2)/2$, where $\hbar\omega_j = \hbar\omega_j$, $j = 0 - 3$ is the energy of state $|j\rangle$. The operator $\mathcal{L}\rho_s$ in Eq. (3) represents the dissipation processes which is given by

$$\begin{aligned} \mathcal{L}\rho_s = & \gamma' (|0\rangle\langle 2|2\rho_s|2\rangle\langle 0| - |2\rangle\langle 2|\rho_s - \rho_s|2\rangle\langle 2|) + \gamma' (|0\rangle\langle 3|2\rho_s|3\rangle\langle 0| - |3\rangle\langle 3|\rho_s - \rho_s|3\rangle\langle 3|) \\ & + \gamma (|1\rangle\langle 2|2\rho_s|2\rangle\langle 1| - |2\rangle\langle 2|\rho_s - \rho_s|2\rangle\langle 2|) + \gamma (|1\rangle\langle 3|2\rho_s|3\rangle\langle 1| - |3\rangle\langle 3|\rho_s - \rho_s|3\rangle\langle 3|) \\ & + \kappa (|1\rangle\langle 3|2\rho_s|2\rangle\langle 1| - |2\rangle\langle 3|\rho_s - \rho_s|2\rangle\langle 3|) + \kappa (|1\rangle\langle 2|2\rho_s|3\rangle\langle 1| - |3\rangle\langle 2|\rho_s - \rho_s|3\rangle\langle 2|) \\ & + \gamma'' (|0\rangle\langle 1|2\rho_s|1\rangle\langle 0| - |1\rangle\langle 1|\rho_s - \rho_s|1\rangle\langle 1|). \end{aligned} \quad (5)$$

The first two terms in Eq. (5) contain the free-space spontaneous decay $\gamma' = \Gamma_0$ [5]. The decay from the two upper states to the lower level is assumed to be the same. The energy difference of states $|2\rangle$ and $|3\rangle$ is rather small, i.e., ω_{32} is only a few Γ_0 , where Γ_0 is the decay rate in free space [12]. The term involving γ'' is very small ($\gamma'' \ll \gamma, \gamma'$) as it arises from a dipole forbidden transition. In this paper we neglect it by taking $\gamma'' = 0$.

The following equations are obtained for the density matrix elements by using Eq. (3) which describes the dynamics of the quantum system

$$\dot{\rho}_{20} = (i\delta + i\frac{\omega_{32}}{2} - \gamma - \gamma')\rho_{20} - \kappa\rho_{30} + i\frac{\Omega_a}{2}(\rho_{00} - \rho_{22}) - i\frac{\Omega_b}{2}e^{-i\phi}\rho_{23}, \quad (6)$$

$$\dot{\rho}_{30} = (i\delta - i\frac{\omega_{32}}{2} - \gamma - \gamma')\rho_{30} - \kappa\rho_{20} + i\frac{\Omega_b}{2}e^{-i\phi}(\rho_{00} - \rho_{33}) - i\frac{\Omega_a}{2}\rho_{32}, \quad (7)$$

$$\dot{\rho}_{23} = (i\omega_{32} - 2\gamma - 2\gamma')\rho_{23} + i\frac{\Omega_a}{2}\rho_{03} - i\frac{\Omega_b}{2}e^{i\phi} - \kappa(\rho_{22} + \rho_{33}), \quad (8)$$

$$\dot{\rho}_{00} = 2\gamma'(\rho_{22} + \rho_{33}) - i\frac{\Omega_a}{2}(\rho_{02} - \rho_{20}) - i\frac{\Omega_b}{2}(\rho_{03}e^{-i\phi} - \rho_{30}e^{i\phi}), \quad (9)$$

$$\dot{\rho}_{22} = -2(\gamma + \gamma')\rho_{22} + i\frac{\Omega_a}{2}(\rho_{02} - \rho_{20}) - \kappa(\rho_{23} + \rho_{32}), \quad (10)$$

$$\dot{\rho}_{33} = -2(\gamma + \gamma')\rho_{33} + i\frac{\Omega_b}{2}(\rho_{03}e^{-i\phi} - \rho_{20}e^{i\phi}) - \kappa(\rho_{23} + \rho_{32}), \quad (11)$$

along with the population conservation $\rho_{00} + \rho_{11} + \rho_{22} + \rho_{33} = 1$ and $\rho_{ij} = \rho_{ji}^*$. The optical coherence corresponding to the probe transition of $|0\rangle \rightarrow |2\rangle$ ($|0\rangle \rightarrow |3\rangle$) is ρ_{20} (ρ_{30}), and the relative phase of the applied fields is denoted by $\phi = \phi_b - \phi_a$. Note that the probe fields are assumed to be very weak so that one can treat them as a perturbation. In the above equations, the parameter κ is the coupling coefficient between states $|2\rangle$ and $|3\rangle$ due to spontaneous emission in a modified anisotropic vacuum [60] (anisotropic Purcell effect) which is responsible for the appearance of quantum interference [61].

The values of γ and κ are given by [10, 11, 62–66]

$$\gamma = \frac{\mu_0\mu^2\bar{\omega}^2}{2\hbar}\hat{\varepsilon}_- \cdot \text{Im}\mathbf{G}(\mathbf{r}, \mathbf{r}; \bar{\omega}) \cdot \hat{\varepsilon}_+, \quad (12)$$

$$\kappa = \frac{\mu_0\mu^2\bar{\omega}^2}{2\hbar}\hat{\varepsilon}_+ \cdot \text{Im}\mathbf{G}(\mathbf{r}, \mathbf{r}; \bar{\omega}) \cdot \hat{\varepsilon}_+. \quad (13)$$

Here, $\mathbf{G}(\mathbf{r}, \mathbf{r}; \bar{\omega})$ [$\bar{\omega} = (\omega_3 + \omega_2)/2 - \omega_1$] describes the dyadic electromagnetic Green's tensor, while \mathbf{r} and μ_0 refer to the position of the quantum emitter and the permeability of vacuum, respectively. One can obtain the values of γ and κ from Eqs. (12) and (13) as [10, 11, 62–66]

$$\gamma = \frac{\mu_0\mu^2\bar{\omega}^2}{2\hbar} \text{Im} [G_{\perp}(\mathbf{r}, \mathbf{r}; \bar{\omega}) + G_{\parallel}(\mathbf{r}, \mathbf{r}; \bar{\omega})] = \frac{1}{2}(\Gamma_{\perp} + \Gamma_{\parallel}), \quad (14)$$

$$\kappa = \frac{\mu_0\mu^2\bar{\omega}^2}{2\hbar} \text{Im} [G_{\perp}(\mathbf{r}, \mathbf{r}; \bar{\omega}) - G_{\parallel}(\mathbf{r}, \mathbf{r}; \bar{\omega})] = \frac{1}{2}(\Gamma_{\perp} - \Gamma_{\parallel}), \quad (15)$$

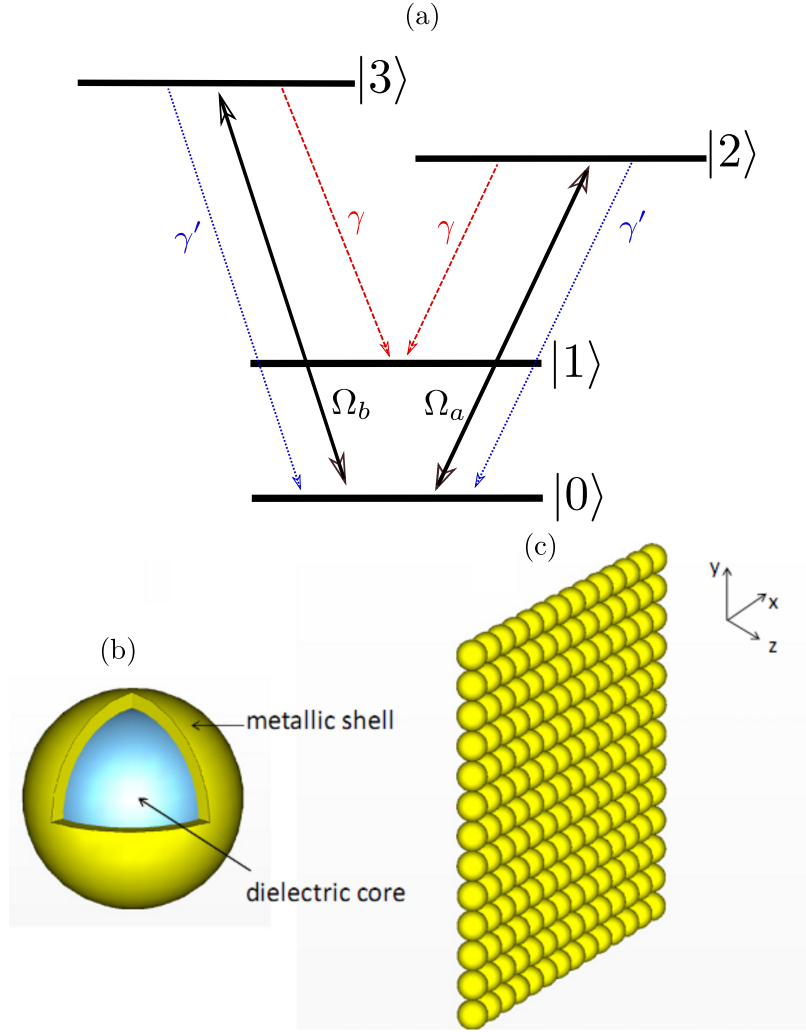


FIG. 1. Schematic diagram of the four-level double-V-type quantum system (a). A metal-coated dielectric nanosphere (b) and a 2D array of such spheres (c).

where $G_{\perp}(\mathbf{r}, \mathbf{r}; \bar{\omega}) = G_{zz}(\mathbf{r}, \mathbf{r}; \bar{\omega})$ and $G_{\parallel}(\mathbf{r}, \mathbf{r}; \bar{\omega}) = G_{xx}(\mathbf{r}, \mathbf{r}; \bar{\omega})$ show components of the electromagnetic Green's tensor, where the symbol $\perp(\parallel)$ refers to a dipole oriented normal, along the z axis (parallel, along the x axis) to the surface of the nanostructure. Let us also define the spontaneous emission rates normal and parallel to the surface as $\Gamma_{\perp, \parallel} = \mu_0 \mu^2 \bar{\omega}^2 \text{Im} [G_{\perp, \parallel}(\mathbf{r}, \mathbf{r}; \bar{\omega})] / \hbar$. The degree of quantum interference is then given by

$$p = (\Gamma_{\perp} - \Gamma_{\parallel}) / (\Gamma_{\perp} + \Gamma_{\parallel}). \quad (16)$$

When $p = \pm 1$ the maximum quantum interference is obtained in spontaneous emission [61]. This is achieved by placing the emitter close to a structure that completely quenches either Γ_{\perp} or Γ_{\parallel} . When the emitter is placed in vacuum, $\Gamma_{\perp} = \Gamma_{\parallel}$ leading $\kappa = 0$, hence no quantum interference occurs in the system.

The plasmonic nanostructure considered here is a 2D array of touching metal-coated silica nanospheres [see Figs. 1(b) and 1(c)]. The dielectric function of the shell is provided by a Drude-type electric permittivity

$$\epsilon(\omega) = 1 - \frac{\omega_p^2}{\omega(\omega + i/\tau)}, \quad (17)$$

where ω_p is the bulk plasma frequency and τ the relaxation time of the conduction-band electrons of the metal. A typical value of the plasma frequency for gold is $\hbar\omega_p = 8.99 \text{ eV}$. This also determines the length scale of the system as $c/\omega_p \approx 22 \text{ nm}$. The dielectric constant of SiO_2 is taken to be $\epsilon = 2.1$. In the calculations we have taken $\tau^{-1} = 0.05\omega_p$. The lattice constant of the square lattice is $a = 2c/\omega_p$ and the sphere radius $S = c/\omega_p$ with core radius $S_c = 0.7c/\omega_p$.

Using this particular choice of sphere/ core radius and lattice constant we achieve maximization of the quantum interference rate p which prerequisite for the observation of the results present below.

For the calculation of the spontaneous decay rates next to the plasmonic nanostructure, we use the layered multiple scattering method [10, 67–69]. We take $\bar{\omega} = 0.632\omega_p$ while the distance between the quantum system and the surface of the plasmonic nanostructure, d , varies from $0.5c/\omega_p$ to c/ω_p . For the results of Γ_{\perp} and Γ_{\parallel} that are used here, we refer to Fig. 3 in Ref. [7]. It is found that Γ_{\parallel} gives significant suppression and its actual value is remarkably lower than the free-space decay rate. In addition, the value of Γ_{\perp} decreases with increasing distance between the quantum system and the plasmonic nanostructure. For distances close to the plasmonic nanostructure, Γ_{\perp} becomes much larger than the free-space decay rate. The value of Γ_{\perp} is larger than the free-space decay rate for distances up to $0.6c/\omega_p$, while for distances between $0.65c/\omega_p$ and c/ω_p the value of Γ_{\perp} becomes lower than the free-space decay rate.

III. CALCULATION OF LINEAR AND NONLINEAR SUSCEPTIBILITIES

In this section we calculate the linear and nonlinear electric susceptibilities for the laser field Ω_a . The probe fields are weak enough and are treated as perturbation to the system under steady-state condition. The method we use extends to third order the method presented in Ref. [70], and it is similar to that used in Ref. [49]. Under the weak-field approximation, the perturbation approach is applied to the density-matrix elements, which is expressed in terms of a perturbative expansion

$$\rho_{ij} = \rho_{ij}^{(0)} + \lambda\rho_{ij}^{(1)} + \lambda^2\rho_{ij}^{(2)} + \lambda^3\rho_{ij}^{(3)} + \dots, \quad (18)$$

where λ is a continuously varying parameter ranging from zero to unity. The constituting terms $\rho_{ij}^{(n)}$ with $n = 1, 2, 3$ are of the n^{th} order in the probe fields. Since the probe fields are assumed to be weak, the zeroth-order solution is $\rho_{00}^{(0)} = 1$, while the other elements $\rho_{ij}^{(0)} = 0$. Replacing Eq. (18) into Eqs. (6)-(11), the equations of motion for the first- and third order density-matrix elements are given by

$$\dot{\rho}_{20}^{(1)} = (i\delta + i\frac{\omega_{32}}{2} - \gamma - \gamma')\rho_{20}^{(1)} - \kappa\rho_{30}^{(1)} + i\frac{\Omega_a}{2}, \quad (19)$$

$$\dot{\rho}_{30}^{(1)} = (i\delta - i\frac{\omega_{32}}{2} - \gamma - \gamma')\rho_{30}^{(1)} - \kappa\rho_{20}^{(1)} + i\frac{\Omega_b}{2}e^{-i\phi}, \quad (20)$$

and

$$\dot{\rho}_{20}^{(3)} = (i\delta + i\frac{\omega_{32}}{2} - \gamma - \gamma')\rho_{20}^{(3)} - \kappa\rho_{30}^{(3)} + i\frac{\Omega_a}{2}(\rho_{00}^{(2)} - \rho_{22}^{(2)}) - i\frac{\Omega_b}{2}e^{-i\phi}\rho_{23}^{(2)}, \quad (21)$$

$$\dot{\rho}_{30}^{(3)} = (i\delta - i\frac{\omega_{32}}{2} - \gamma - \gamma')\rho_{30}^{(3)} - \kappa\rho_{20}^{(3)} + i\frac{\Omega_b}{2}e^{-i\phi}(\rho_{00}^{(2)} - \rho_{33}^{(2)}) - i\frac{\Omega_a}{2}\rho_{32}^{(2)}. \quad (22)$$

After some lengthy but straightforward algebra we get

$$\rho_{20}^{(1)} = i\frac{\Omega_a}{2}S_1 - i\kappa\frac{\Omega_b}{2}e^{-i\phi}S_2, \quad (23)$$

$$\rho_{30}^{(1)} = i\frac{\Omega_b}{2}e^{-i\phi}S_3 - i\kappa\frac{\Omega_a}{2}S_2. \quad (24)$$

and

$$\rho_{20}^{(3)} = -a_2\kappa - a_1(i\delta - i\frac{\omega_{32}}{2} - \gamma - \gamma'). \quad (25)$$

$$\rho_{30}^{(3)} = -a_1\kappa - a_2(i\delta + i\frac{\omega_{32}}{2} - \gamma - \gamma'), \quad (26)$$

where

$$S_1 = \frac{(-i\delta + i\frac{\omega_{32}}{2} + \gamma + \gamma')}{(-i\delta + i\frac{\omega_{32}}{2} + \gamma + \gamma')(-i\delta - i\frac{\omega_{32}}{2} + \gamma + \gamma') - \kappa^2}, \quad (27)$$

$$S_2 = \frac{1}{(-i\delta + i\frac{\omega_{32}}{2} + \gamma + \gamma')(-i\delta - i\frac{\omega_{32}}{2} + \gamma + \gamma') - \kappa^2}, \quad (28)$$

$$S_3 = \frac{(-i\delta - i\frac{\omega_{32}}{2} + \gamma + \gamma')}{(-i\delta + i\frac{\omega_{32}}{2} + \gamma + \gamma')(-i\delta - i\frac{\omega_{32}}{2} + \gamma + \gamma') - \kappa^2}, \quad (29)$$

and

$$a_1 = \frac{-i\frac{\Omega_a}{2}(\rho_{00}^{(2)} - \rho_{22}^{(2)}) - i\frac{\Omega_b}{2}e^{-i\phi}\rho_{23}^{(2)}}{(-i\delta + i\frac{\omega_{32}}{2} + \gamma + \gamma')(-i\delta - i\frac{\omega_{32}}{2} + \gamma + \gamma') - \kappa^2}, \quad (30)$$

$$a_2 = \frac{-i\frac{\Omega_b}{2}e^{-i\phi}(\rho_{00}^{(2)} - \rho_{33}^{(2)}) - i\frac{\Omega_a}{2}\rho_{32}^{(2)}}{(-i\delta + i\frac{\omega_{32}}{2} + \gamma + \gamma')(-i\delta - i\frac{\omega_{32}}{2} + \gamma + \gamma') - \kappa^2}. \quad (31)$$

The second-order density matrix elements of Eqs. (25) and (26) featured in Eqs. (30) and (31) can be solved to obtain the steady-state solutions $\rho_{ij}^{(2)}$ (see Appendix A). In order to obtain the linear susceptibility $\chi^{(1)}$ and the third-order nonlinear susceptibility $\chi^{(3)}$, the susceptibility is assumed to be written as

$$\chi \approx \chi^{(1)} + 3\chi^{(3)}E_a^2/4. \quad (32)$$

Then, using

$$\chi(\delta) = \frac{\sqrt{2}N\mu'}{\varepsilon_0 E_a} \rho_{20}, \quad (33)$$

and expanding ρ_{20} in perturbation series we get

$$\chi^{(1)}(\delta) = \frac{\sqrt{2}N\mu'}{\varepsilon_0 E_a} \rho_{20}^{(1)} = \frac{N\mu'^2}{\varepsilon_0 \hbar} \frac{\rho_{20}^{(1)}}{\Omega_a}, \quad (34)$$

and

$$\chi^{(3)}(\delta)E_a^2 = \frac{4N\mu'^2}{3\varepsilon_0 \hbar} \frac{\rho_{20}^{(3)}}{\Omega_a}. \quad (35)$$

Substituting Eqs. (27)-(31) [and using Eqs. (A1)-(A7)] into equations (23), (25) and defining $x = \frac{\Omega_b}{\Omega_a}$, Eqs. (34) and (35) become

$$\chi^{(1)}(\delta) = \frac{N\mu'^2}{\varepsilon_0 \hbar} \frac{-i\kappa A + B(\delta - \frac{\omega_{32}}{2} + i\gamma + i\gamma')}{(-i\delta + i\frac{\omega_{32}}{2} + \gamma + \gamma')(-i\delta - i\frac{\omega_{32}}{2} + \gamma + \gamma') - \kappa^2}, \quad (36)$$

and

$$\chi^{(3)}(\delta) = \frac{2N\mu'^4}{3\varepsilon_0 \hbar^3} \frac{-i\kappa C + D(\delta - \frac{\omega_{32}}{2} + i\gamma + i\gamma')}{(-i\delta + i\frac{\omega_{32}}{2} + \gamma + \gamma')(-i\delta - i\frac{\omega_{32}}{2} + \gamma + \gamma') - \kappa^2}, \quad (37)$$

where here ε_0 is the vacuum permittivity and N is the density of the quantum systems, where A , B , C and D are defined in Appendix B.

The refraction part of the third-order susceptibility $\chi^{(3)}$ corresponds to the Kerr nonlinearity, while its imaginary part determines the nonlinear absorption. The real and imaginary parts of $\chi^{(1)}$ represent the linear dispersion and absorption, respectively. From Eqs. (36) and (37) one can clearly see that the expressions for the linear and nonlinear susceptibility are very similar in form with the only difference in their coefficients. So, one may expect to observe similar variation of the curves for $\chi^{(1)}$ and $\chi^{(3)}$ with the difference in their magnitude. However, this does not happen as the coefficients of the linear susceptibility does not depend on the detuning δ and the coefficients of the nonlinear susceptibility depends strongly on the detuning δ , so the frequency variation of the two susceptibilities is different. In addition, one can see that the linear and nonlinear susceptibilities $\chi^{(1)}$ and $\chi^{(3)}$ can be controlled by the system parameters such as the relative phase of applied fields ϕ .

IV. PHASE DEPENDENT NONLINEAR OPTICAL EFFECTS

Next we study the nonlinear response of the quantum system to the probe field Ω_a for weak intensities via numerical simulation (the linear and nonlinear susceptibilities are plotted in units of $\frac{N\mu'^2}{\varepsilon_0 \hbar}$ and $\frac{2N\mu'^4}{3\varepsilon_0 \hbar^3}$, respectively). Figure 2 shows the real and imaginary parts of $\chi^{(1)}$ and $\chi^{(3)}$ as a function of the detuning δ when the quantum system is in vacuum, i.e., without the plasmonic nanostructure. We assume that the two upper levels are degenerate ($E_2 = E_3$

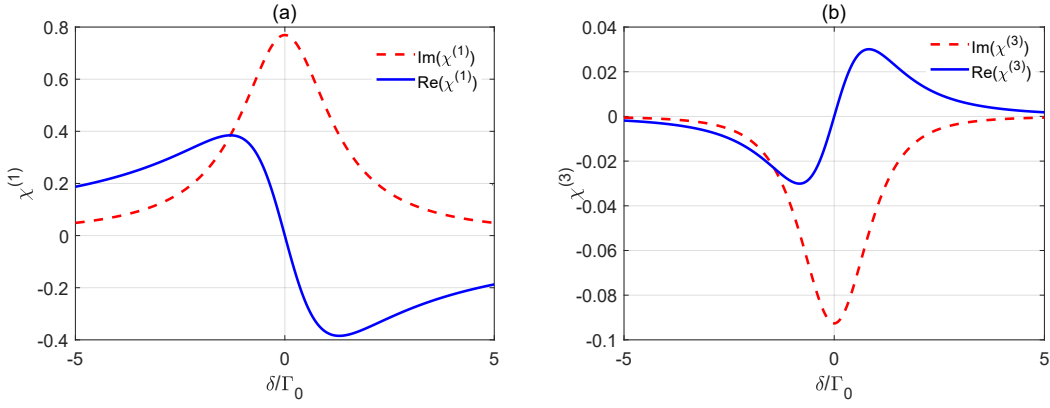


FIG. 2. (a) Linear susceptibility $\chi^{(1)}$ and (b) nonlinear susceptibility $\chi^{(3)}$ of the quantum system for the weak probe field Ω_a in arbitrary units as a function of the probe detuning δ in the absence of the plasmonic nanostructure. We have assumed that $\omega_{32} = 0$, $\gamma' = 0.3\Gamma_0$ and $\gamma'' = 0$.

leading to $\omega_{32} = 0$). This assumption significantly simplifies Eqs. (36) and (37) giving (for $\delta = 0$) analytical expressions for the linear as well as nonlinear absorption and dispersion coefficients (see Appendix C). The typical linear [Fig. 2(a)] and nonlinear [Fig. 2(b)] susceptibility spectra for this case are such that that the medium experiences strong linear and nonlinear absorption at $\delta = 0$. This is already expected from Eqs. (36) and (37) when the quantum system is not near the plasmonic nanostructure ($\kappa = 0$ and $\gamma = \Gamma_0$). Setting $\kappa = 0$ and $\gamma = \Gamma_0$ into Eqs. (C1)- (C4), one can simplify these equations giving the resonant linear and nonlinear absorption and dispersion coefficients

$$Im(\chi^{(1)}(\delta = 0)) = \frac{N\mu'^2}{\varepsilon_0\hbar} \frac{1}{(\Gamma_0 + \gamma')}, \quad (38)$$

$$Re(\chi^{(1)}(\delta = 0)) = 0, \quad (39)$$

$$Im(\chi^{(3)}(\delta = 0)) = \frac{2N\mu'^4}{3\varepsilon_0\hbar^3} \frac{1 - x^2}{8(\Gamma_0 + \gamma')^2}, \quad (40)$$

$$Re(\chi^{(3)}(\delta = 0)) = 0. \quad (41)$$

On exact resonance, the Kerr nonlinearity is zero for the quantum system [see Fig. 2(b) and (Eq. (41))], while its magnitude is very weak around the resonance accompanied by the linear (Eq. (38)) and nonlinear (Eq. (40)) absorption. The slope of linear dispersion is negative around zero probe detuning suggesting superluminal light propagation [Fig. 2(a)]. We note that no phase dependence is obtained in this case.

The linear and nonlinear optical properties of the quantum system are very different when the quantum system is placed near the plasmonic nanostructure. In Figs. 3(a) and (c) where the quantum system is near the plasmonic nanostructure, we obtain a gain dip in the linear absorption profile at $\delta = 0$. The slope of linear dispersion becomes positive, indicating slow light condition. As shown in Figs. 3(b) and (d), the enhanced Kerr nonlinearity appears inside the linear gain regions. The maximal Kerr nonlinearity around resonance is enhanced by almost four times when the distance between the quantum emitter and the nanostructure increases from $d = 0.3c/\omega_p$ [Figs. 3(b)] to $d = 0.6c/\omega_p$ [Figs. 3(d)].

As illustrated in Figs. 4, both $\chi^{(1)}$ and $\chi^{(3)}$ are observed to behave differently for large distances of the quantum system from the plasmonic nanostructure. We observe that linear gain changes to a double-peaked absorption spectrum for $d = 0.7c/\omega_c$ (Fig. 4(a)). The Kerr nonlinearity find its maximal value around the zero probe field detuning [Fig. 4(b)]. In Fig. 4(d), nonlinear gain takes also place in the medium by altering the distance d (which leads to the change in values of Γ_{\perp} and Γ_{\parallel}). We obtain different behaviors of $\chi^{(1)}$ and $\chi^{(3)}$. This is the main reason for appearance of gain or absorption in the quantum system as demonstrated in Figs. 3 and Figs. 4. The minima of linear

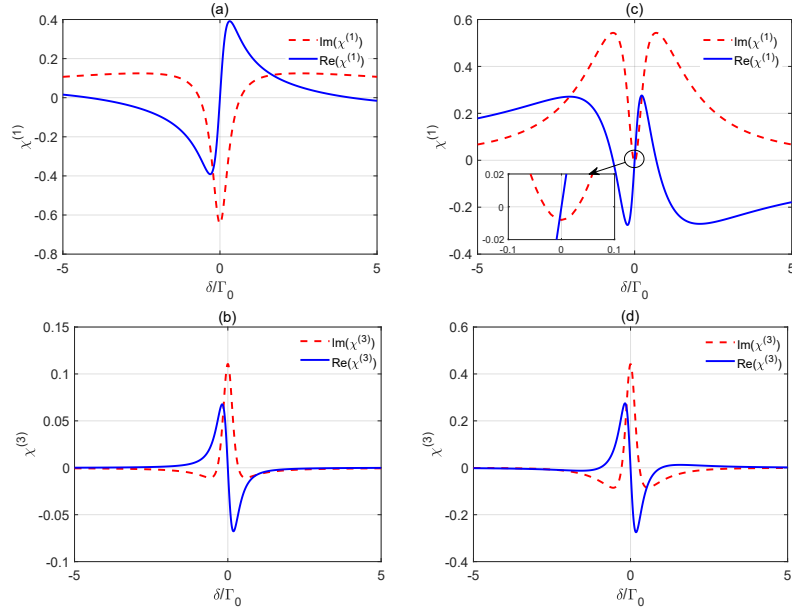


FIG. 3. (a,c) Linear susceptibility $\chi^{(1)}$ and (b,d) nonlinear susceptibility $\chi^{(3)}$ of the quantum system for the weak probe field Ω_a in arbitrary units as a function of the probe detuning δ in the presence of the plasmonic nanostructure. We take here $\omega_{32} = 0$, $\gamma' = 0.3\Gamma_0$, $\gamma'' = 0$, $x = 1.5$, $\phi = 0$, $\bar{\omega} = 0.632\omega_p$, and $d = 0.3c/\omega_p$ (a,b), $d = 0.6c/\omega_p$ (c,d).

(and nonlinear) absorption or gain in Figs. 3 and 4 are given by Eqs. (C1) (and (C3)). One can show from Eqs. (C1), that the gain is present at $\delta = 0$ when (Figs. 3)

$$\Omega_b > \frac{2\gamma' + \Gamma_{\perp} + \Gamma_{\parallel}}{(\Gamma_{\perp} - \Gamma_{\parallel}) \cos \phi} \Omega_a, \quad (42)$$

while absorption takes place when when (Figs. 4)

$$\Omega_b < \frac{2\gamma' + \Gamma_{\perp} + \Gamma_{\parallel}}{(\Gamma_{\perp} - \Gamma_{\parallel}) \cos \phi} \Omega_a. \quad (43)$$

Equations. (36) and (37) and their corresponding coefficients in Appendix B prove that in the presence of the plasmonic nanostructure, the linear and nonlinear susceptibilities are sensitive to the relative phase of the weak probe fields. Figures. 5 and 6 illustrate the dependence of $\chi^{(1)}$ and $\chi^{(3)}$ on ϕ when the quantum system is placed at a distance $d = 0.4c/\omega_p$ from the surface of the plasmonic nanostructure. The strong variation of linear and nonlinear absorption and dispersion profiles for different values of ϕ is obvious. In particular, for $\phi = 0$ the maximal of Kerr nonlinearity is placed in a region of linear gain around $\delta = 0$. Subluminal response takes place in this situation on resonance [see Figs. 5(a) and 6(a)]. When ϕ becomes π , a strong absorption instead of gain appears at line center for the $\chi^{(1)}$ profile, as can be seen in Fig. 5(c). Such a phase sensitive gain and absorption is well understood through Eqs. (42) and (43). In both cases, the value of the Kerr index at exact resonance is zero. According to Eq. (C4), for $\phi = 0$ and $\phi = \pi$, both sine terms in Eq. (C4) vanish leading to zero Kerr nonlinearity on resonance. It should be mentioned that a nonzero resonant Kerr nonlinearity can be obtained for $\phi = \pi/2$ [Fig. 6(b)] and $\phi = 3\pi/2$ [Fig. 6(d)].

The results obtained here may suggest a tunable control over the Kerr nonlinearity of the quantum system near the plasmonic nanostructure by using the relative phase of the applied fields. In Fig. 7 we present an example of the variation of the Kerr nonlinearity spectra for different distances of the quantum system from the plasmonic nanostructure, $d = 0.2c/\omega_p$ (dot line), $d = 0.5c/\omega_p$ (dash line), $d = 0.7c/\omega_p$ (solid line). A wide range of tunability can be observed over the refractive part of third-order nonlinear susceptibility $\chi^{(3)}$ spectra just by adjusting the relative phase parameter. We find that the whole profile for Kerr nonlinearity is enhanced for larger distances due to the reduction of both Γ_{\perp} and Γ_{\parallel} reduces by distance. The nonlinear dispersion becomes zero at $\phi = n\pi$, while it obtains its maximal amplitude for $\phi = n\pi/2$. It also changes from negative to positive and back to positive as the relative phase changes from 0 to 2π .

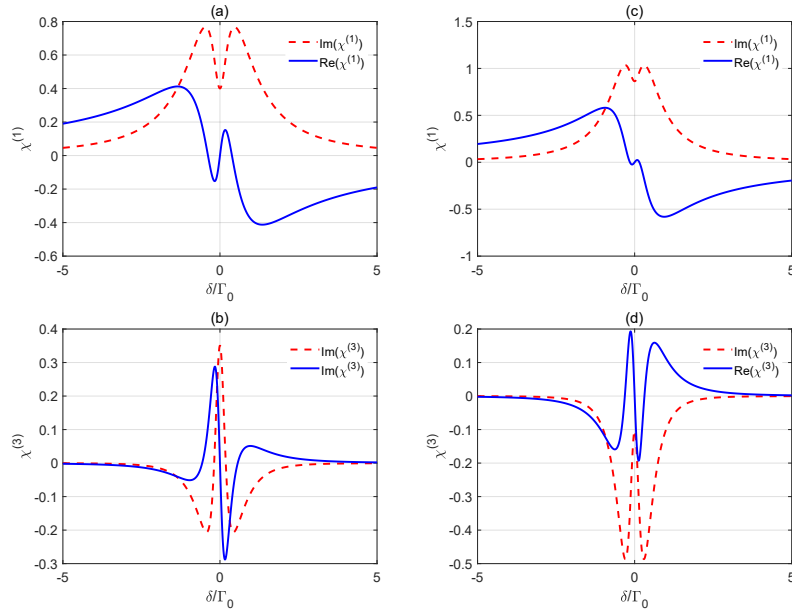


FIG. 4. (a,c) Linear susceptibility $\chi^{(1)}$ and (b,d) nonlinear susceptibility $\chi^{(3)}$ of the quantum system for the weak probe field Ω_a in arbitrary units as a function of the probe detuning δ in the presence of the plasmonic nanostructure. We take here $\omega_{32} = 0$, $\gamma' = 0.3\Gamma_0$, $\gamma'' = 0$, $x = 1.5$, $\phi = 0$, $\bar{\omega} = 0.632\omega_p$, and $d = 0.7c/\omega_p$ (a,b), $d = 0.8c/\omega_p$ (c,d).

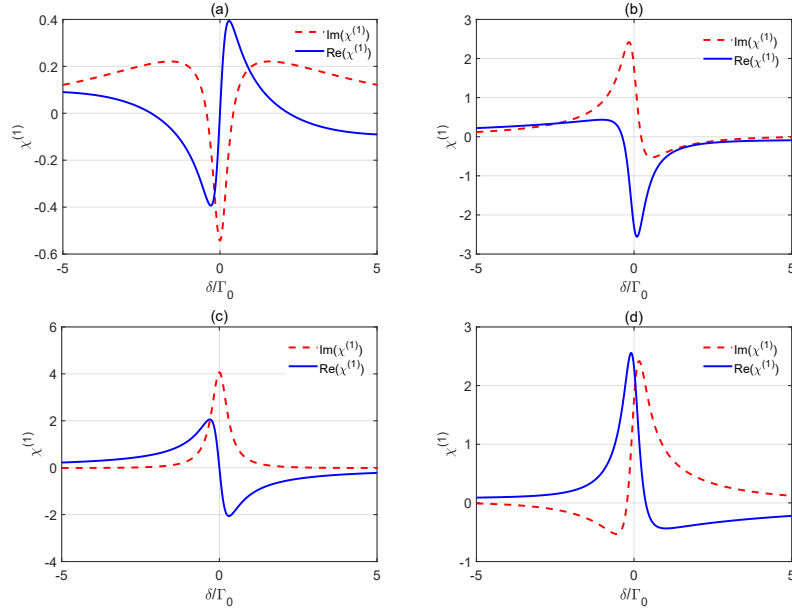


FIG. 5. Linear susceptibility $\chi^{(1)}$ of the quantum system for the weak probe field Ω_a in arbitrary units as a function of the probe detuning δ in the presence of the plasmonic nanostructure. We have assumed that $\omega_{32} = 0$, $\gamma' = 0.3\Gamma_0$, $\gamma'' = 0$, $x = 1.5$, $\phi = 0$, $\bar{\omega} = 0.632\omega_p$, $d = 0.4c/\omega_p$ and (a), $\phi = 0$, (b), $\phi = \pi/2$, (c) $\phi = \pi$, and (d) $\phi = 3\pi/2$.

V. SPATIALLY STRUCTURED OPTICAL EFFECTS

Up to now no assumption has been made about the spatial profile of laser fields. Next, we will consider the case where the incident field possesses a nontrivial structural profile which, however, is almost unaffected by the plasmonic nanostructure (marginal reflection and absorption) as it is tuned to the resonant frequencies of the lower V-type subsystem which lie well beyond, say well above, the surface-plasmon bands of the nanostructure in which case the nanostructure is almost transparent to the impinging structured laser field. Since, the position of the quantum is kept

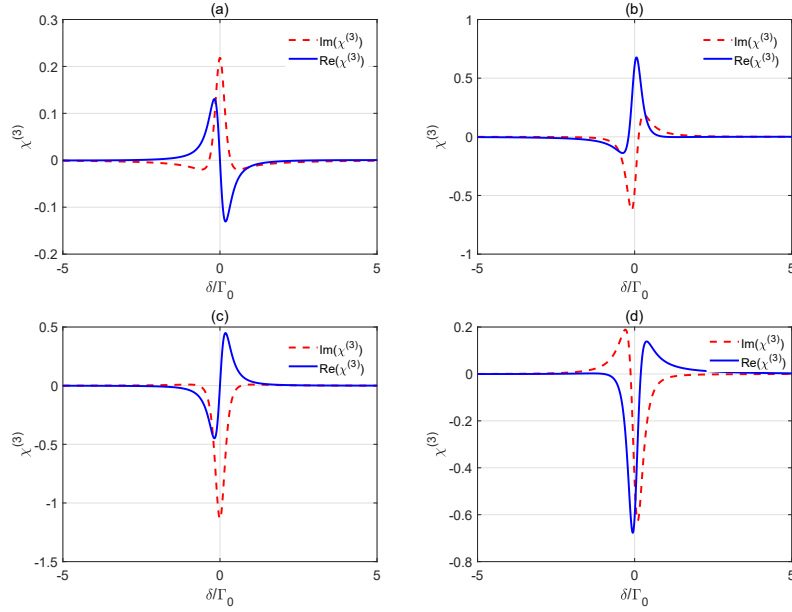


FIG. 6. Nonlinear susceptibility $\chi^{(3)}$ of the quantum system for the weak probe field Ω_a in arbitrary units as a function of the probe detuning δ in the presence of the plasmonic nanostructure. We have assumed that $\omega_{32} = 0$, $\gamma' = 0.3\Gamma_0$, $\gamma'' = 0$, $x = 1.5$, $\phi = 0$, $\bar{\omega} = 0.632\omega_p$, $d = 0.4c/\omega_p$ and (a), $\phi = 0$, (b), $\phi = \pi/2$, (c) $\phi = \pi$, and (d) $\phi = 3\pi/2$.

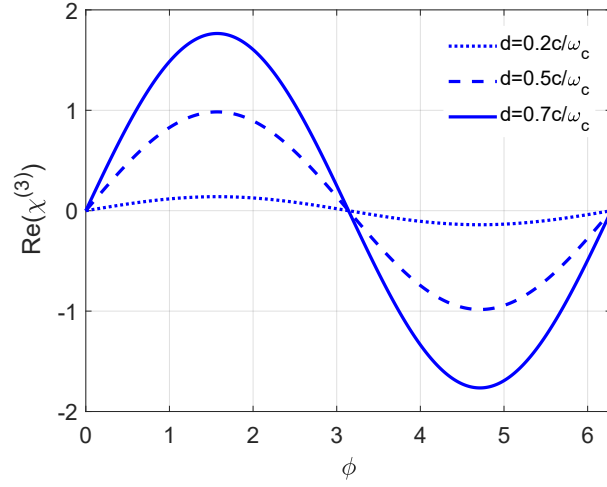


FIG. 7. The refractive part of third-order nonlinear susceptibility $Re(\chi^{(3)})$ (Kerr nonlinearity) of the quantum system for the weak probe field Ω_a in arbitrary units as a function of the relative phase ϕ for different distances from the plasmonic nanostructure $d = 0.2c/\omega_p$ (dot line), $d = 0.5c/\omega_p$ (dash line), $d = 0.7c/\omega_p$ (solid line). We take here $\omega_{32} = 0$, $\gamma' = 0.3\Gamma_0$, $\gamma'' = 0$, $x = 1.5$, $\phi = 0$, $\bar{\omega} = 0.632\omega_p$.

fixed, i.e. right opposite the center of the nanosphere, we will study the role of the position of the quantum system within the structured-field landscape, which, given the fixed position of the quantum system, is translated into the dependence of the applied structured field relative to the nanostructure.

We assume that the probe field Ω_b has an orbital angular momentum $\hbar l$ along the propagation axis z [71]. In this case, the vortex probe field Ω_b is characterized by the Rabi frequency

$$\Omega_b = A_b \exp(il\Phi). \quad (44)$$

For a Laguerre-Gaussian (LG) doughnut beam we may write the amplitude of a vortex beam A_b as

$$A_b(\varrho) = |\Omega_b| \left(\frac{\varrho}{w}\right)^{|l|} \exp\left(-\frac{\varrho^2}{w^2}\right), \quad (45)$$

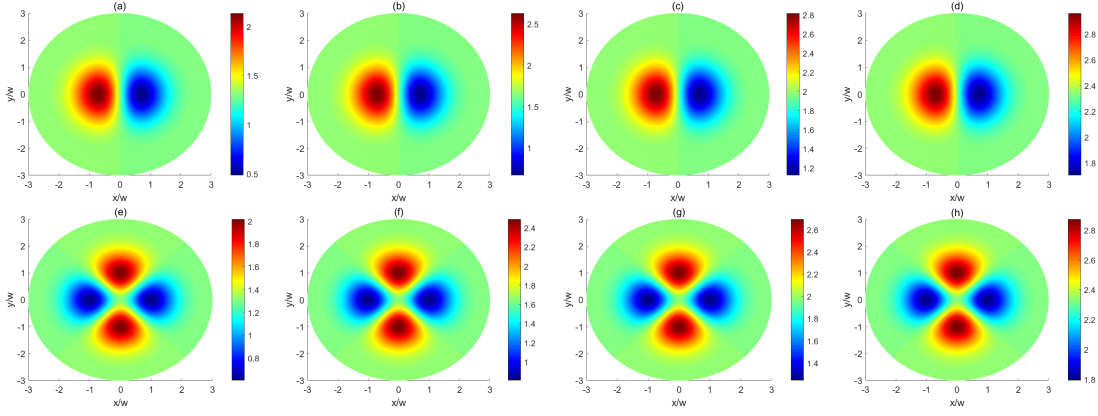


FIG. 8. Spatially structured linear absorption $Im(\chi^{(1)})$ profiles of the probe beam Ω_a in arbitrary units, in the presence of the plasmonic nanostructure and for different values of the distance d of the quantum system from the plasmonic nanostructure: $d = 0.1c/\omega_c$ (a,e), $d = 0.3c/\omega_p$ (b,f), $d = 0.6c/\omega_p$ (c,g) and $d = 0.8c/\omega_p$ (d,h). Here, the winding number is $l = 1$ for (a,b,c,d) and $l = 2$ (e,f,g,h), while the other parameters are $\delta = 0$, $\omega_{32} = 0$, $|\frac{\Omega_b}{\Omega_a}| = 1.5$, $\bar{\omega} = 0.632\omega_p$, $\gamma' = 0.3\Gamma_0$ and $\gamma'' = 0$.

where $\Phi = \tan^{-1}(y/x)$ is the azimuthal angle, x and y are transverse directions, $\rho = \sqrt{x^2 + y^2}$ represents the distance from the vortex core (cylindrical radius), w denotes the beam waist parameter, and $|\Omega_b|$ is the strength of the vortex beam. The Rabi frequency of the other probe field does not have a vortex and is given by

$$\Omega_a = |\Omega_a|. \quad (46)$$

In this case, Eqs. (19)-(31) for the evolution of the system and their corresponding coefficients featured in Appendix A remain the same, with the only difference that ϕ changes to $l\Phi$. In addition, Eqs. (36) and (37) will describe the azimuthally varying linear and nonlinear susceptibilities under the transformation $\phi \rightarrow l\Phi$, yet one needs to perform also the transformation $x \rightarrow X(\frac{\rho}{w})^{|l|} \exp(-\frac{\rho^2}{w^2})$, where $X = \frac{|\Omega_b|}{|\Omega_a|}$ in the corresponding coefficients given in Appendix B. This allows to study the azimuthal modulation of the linear and nonlinear response of a weak non-vortex probe field Ω_a at weak intensity regime.

We will consider a situation where the laser fields are at exact resonance with the corresponding transitions ($\delta = 0$). We also assume that the quantum system is degenerate ($\omega_{32} = 0$). In this case, the imaginary part of Eq. (36) for the linear absorption of probe field Ω_a simplifies to

$$Im(\chi^{(1)}(\delta = 0)) = \frac{N\mu'^2}{\varepsilon_0\hbar} \frac{(\gamma + \gamma') - \kappa A \cos(l\Phi)}{(\gamma + \gamma')^2 - \kappa^2}. \quad (47)$$

Eq. (47) implies that the linear absorption of the probe field Ω_a can be influenced by the vortex probe beam Ω_b through the term $\kappa A \cos(l\Phi)$. This term contains a phase factor $l\Phi$ accounting for the spatial variation of the probe absorption. It is indeed the existence of the quantum interference term κ , which makes the quantum system sensitive to the azimuthal phase, resulting in the spatially-dependent linear absorption when the quantum system is near the plasmonic nanostructure ($d \neq 0$), as shown in Fig. 8.

Fig. 8 demonstrates the resulting absorption spectra for different values of the distance d . The results are presented in Figs. 8 for two different vorticities $l = 1$ [Figs. 8 (a,b,c,d)] and $l = 2$ [Figs. 8 (e,f,g,h)]. From Fig. 8, we observe that the linear absorption increases with the distance d for the whole region of transverse spatial profile. The spatially structured absorption profiles oscillate sinusoidally in the presence of the plasmonic nanostructure [see also Eq. (47)].

Eq. (47) implies that the linear absorption of the system for the transition $|0\rangle \leftrightarrow |2\rangle$ of the quantum system near the plasmonic nanostructure can be manipulated through the winding number l (OAM number). The l factor in the cosine term of Eq. (47) governs the number of absorption peaks (or dips) in the transverse ($x-y$) plane. The periodic oscillatory behavior of the absorption profile in the transverse plane for a given value of distance $d = 0.4c/\omega_c$ but different OAM numbers $l = 1 - 6$ is observed in Fig. 9. Because of the angular dependence, the spatially structured absorption profile displays a l -fold symmetry. The number of absorption peaks (or dips) increases with larger winding number l . As a result, one can easily distinguish an unknown vorticity of a vortex probe beam Ω_b solely by counting the bright spots appearing in the absorption profile of the probe field Ω_a . Furthermore, the maximum of the linear absorption curve is enhanced in some regions of the transverse plane by increasing the winding number, while gain appears in some other regions.

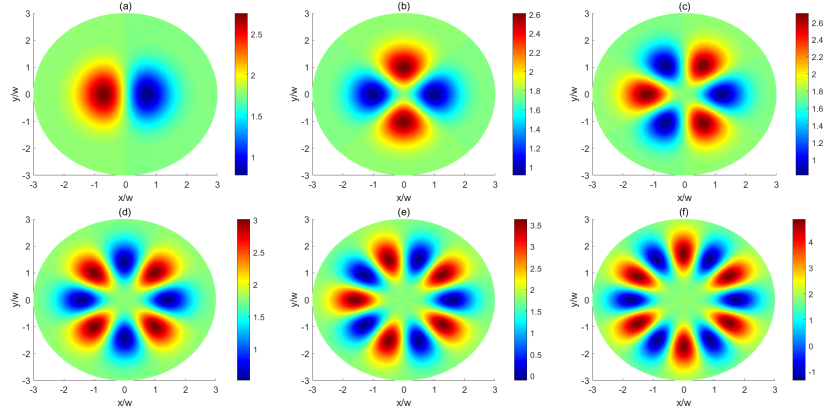


FIG. 9. Spatially structured linear absorption $Im(\chi^{(1)})$ profiles of the probe beam Ω_a in arbitrary units, in the presence of the plasmonic nanostructure and for different winding $l = 1(a) - l = 6 (f)$. Here, $d = 0.4c/\omega_p$ and the other parameters are the same as Fig. 8.

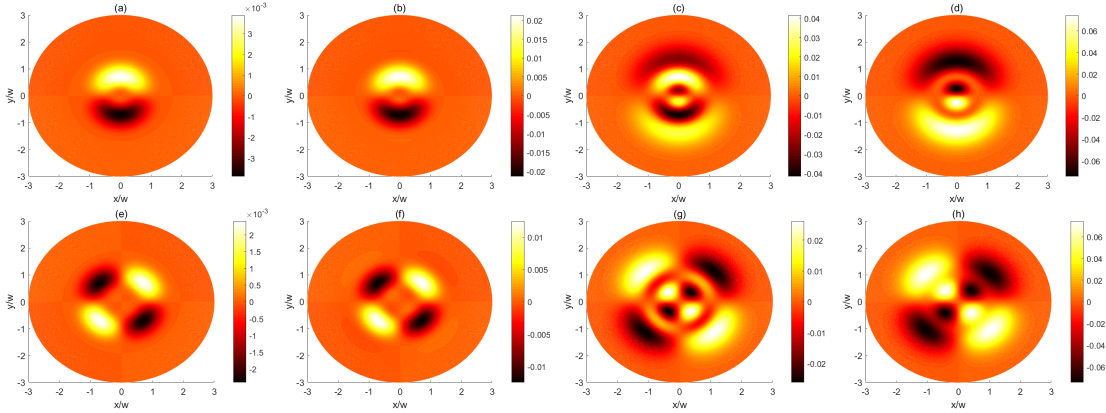


FIG. 10. Spatially structured Kerr nonlinearity $Re(\chi^{(3)})$ profiles of the probe beam Ω_a in arbitrary units, in the presence of the plasmonic nanostructure and for different values of distance d of the quantum system from the plasmonic nanostructure: $d = 0.1c/\omega_p$ (a,e), $d = 0.3c/\omega_p$ (b,f), $d = 0.6c/\omega_p$ (c,g) and $d = 0.8c/\omega_p$ (d,h). Here, the winding number is $l = 1$ for (a,b,c,d) and $l = 2$ (e,f,g,h), and the other parameters are the same as Fig. 8.

In Figs. 10 and 11, we show the Kerr nonlinearity of the medium as a function of the transverse directions x and y . As can be seen from Fig. 10, the spatially-dependent Kerr nonlinearity is very sensitive to the distance from the plasmonic nanostructure. The Kerr nonlinearity is remarkably enhanced when increasing the distance parameter d . In particular, the maximal Kerr nonlinearity is enhanced by almost 10 times when we increase d from $0.1c/\omega_p$ [Figs. 10 (a,e)] to $0.3c/\omega_p$ [Figs. 10 (b,f)]. Larger values of d mean higher values of the Kerr nonlinearity. However, the maximal of Kerr nonlinearity is distributed to other regions of the transverse plane [see (Figs. 10 (c,d,g,f))].

Finally in Fig. 11 we display how the winding number affects the Kerr nonlinearity of the system. The results show a l -fold symmetry of the Kerr nonlinearity. Moreover, very large position-dependent Kerr nonlinearities can be achieved just by increasing the winding number l .

Note that we have assumed the quantum system to be degenerated ($\omega_{32} = 0$). We have also performed calculations with non-zero ω_{32} (not shown here). We have observed a similar qualitative response for linear and nonlinear susceptibilities for $\omega_{32} \neq 0$ with that presented above with $\omega_{32} = 0$. Yet, both the linear and nonlinear susceptibilities reduce in magnitude as ω_{32} increases.

VI. CONCLUDING REMARKS

We have studied the third-order nonlinear susceptibility behavior of a four-level closed-loop double-V-type quantum system near a plasmonic nanostructure. In the system under study, the lower V-type transition interacts with the free-space vacuum, while the upper V-type transition is affected by the interaction with localized surface plasmons. Two

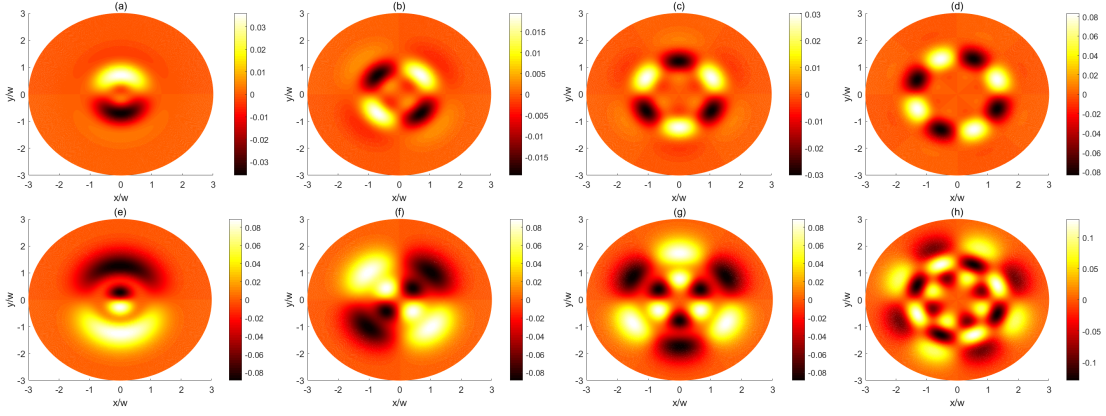


FIG. 11. Spatially structured Kerr nonlinearity $Re(\chi^{(3)})$ profiles of the probe beam Ω_a in arbitrary units, in the presence of the plasmonic nanostructure and for different winding $l = 1$ (a,e), $l = 2$ (b,f), $l = 3$ (c,g) and $l = 4$ (d,h). Here, $d = 0.4c/\omega_p$ (a,b,c,d), $d = 0.9c/\omega_p$ (e,f,g,h), and the other parameters are the same as Fig. 8.

orthogonal circularly polarized laser fields with the same frequency and different phases and electric field amplitudes act on both transitions of the lower V-type system. A 2D array of metal-coated dielectric nanospheres is considered as a plasmonic nanostructure for which the relevant decay rates are calculated by a rigorous electromagnetic Green tensor technique.

We have shown that the presence of the plasmonic nanostructure significantly modifies the nonlinear response of the system resulting in large enhancement of the Kerr nonlinearity. In particular, the Kerr nonlinearity can be remarkably modified by increasing the distance of the quantum system from the plasmonic nanostructure. Phase control of the Kerr nonlinearity has also been discussed for such a quantum system. A wide range of tunability has been observed over the Kerr nonlinear response through the effect of the relative phase. Such a mechanism for phase control of the Kerr nonlinearity may be realized by the state-of-the-art nanomethods and it may find application in on-chip photonic nonlinear devices.

We have also analyzed the light-matter interaction of the same system when one probe field carries an optical vortex, and another probe field has no vortex. Because of the creation of quantum interference, the linear and nonlinear susceptibility of the nonvortex probe beam depends on the azimuthal angle and the vorticity of the twisted probe beam. This is different from an open double-V type quantum system interacting with free-space vacuum, because no quantum interference occurs in that case. Thanks to the angular dependence of the optical susceptibility for the quantum system we can obtain regions of high or low transmission as well as regions of large or small nonlinearity. We have then investigated the effect of different external parameters of the system, i.e., the surface of plasmonic nanostructure and the vorticity of twisted probe beam. The results obtained here can be used in optoelectronics and quantum information processing and may find potential applications in storage of high-dimensional optical information in phase dependent quantum memories.

ACKNOWLEDGEMENTS

We acknowledge useful discussions with S.H. Asadpour.

Appendix A: Explicit expressions for $\rho_{ij}^{(2)}$

The expressions for the steady-state solutions $\rho_{ij}^{(2)}$ are:

$$\rho_{11}^{(2)} = -\frac{(r+s)}{2\gamma'}, \quad (\text{A1})$$

$$\rho_{22}^{(2)} = \frac{2\gamma'\kappa r + \kappa\gamma(r+s)}{4\gamma'\kappa(\gamma + \gamma')}, \quad (\text{A2})$$

$$\rho_{33}^{(2)} = \frac{2\gamma'\kappa s + \kappa\gamma(r+s)}{4\gamma'\kappa(\gamma + \gamma')}, \quad (\text{A3})$$

$$\rho_{23}^{(2)} = \frac{\kappa(r+s) - 2\gamma't}{2\gamma'(i\omega_{32} - 2\gamma - 2\gamma')}, \quad (\text{A4})$$

and $\rho_{00}^{(2)} = 0$, where

$$t = \frac{i\Omega_a}{2} \left(-i\frac{\Omega_b}{2} e^{i\phi} S_3^* + i\kappa\frac{\Omega_a}{2} S_2^* \right) - i\frac{\Omega_b}{2} e^{i\phi} \left(i\frac{\Omega_a}{2} S_1 - i\kappa\frac{\Omega_b}{2} e^{-i\phi} S_2 \right), \quad (\text{A5})$$

$$r = \frac{i\Omega_a}{2} \left(\left(-i\frac{\Omega_a}{2} S_1^* + i\kappa\frac{\Omega_b}{2} e^{i\phi} S_2^* \right) - \left(i\frac{\Omega_a}{2} S_1 - i\kappa\frac{\Omega_b}{2} e^{-i\phi} S_2 \right) \right), \quad (\text{A6})$$

$$s = \frac{i\Omega_b}{2} \left(\left(-i\frac{\Omega_b}{2} e^{i\phi} S_3^* + i\kappa\frac{\Omega_a}{2} S_2^* \right) e^{-i\phi} - \left(i\frac{\Omega_b}{2} e^{-i\phi} S_3 - i\kappa\frac{\Omega_a}{2} S_2 \right) e^{i\phi} \right). \quad (\text{A7})$$

Appendix B: Explicit expressions for A , B , C , D , and f_i

The expressions for the coefficients A , B , C and D are:

$$A = e^{-i\phi} x, \quad (\text{B1})$$

$$B = 1, \quad (\text{B2})$$

$$C = \frac{1}{8} \left[-\frac{2\gamma'f_1 + \gamma f_2}{4\gamma'(\gamma + \gamma')} - \frac{\kappa f_3 + 2\gamma'f_4}{2\gamma'(-i\omega_{32} - 2\gamma - 2\gamma')} \right], \quad (\text{B3})$$

$$D = \frac{1}{8} \left[-\frac{2\gamma'f_5 + \gamma f_6}{4\gamma'(\gamma + \gamma')} - \frac{\kappa f_7 + 2\gamma'f_8}{2\gamma'(i\omega_{32} - 2\gamma - 2\gamma')} \right], \quad (\text{B4})$$

with

$$f_1 = -x^3 e^{-i\phi} (S_3 + S_3^*) + x^2 \kappa e^{-2i\phi} S_2^* + \kappa x^2 S_2, \quad (\text{B5})$$

$$f_2 = -x e^{-i\phi} (S_1 + S_1^*) + \kappa x^2 (S_2 + S_2^*) - x^3 e^{-i\phi} (S_3 + S_3^*) - \kappa x^2 e^{-2i\phi} (S_2 - S_2^*), \quad (\text{B6})$$

$$f_3 = -(S_1 + S_1^*) + \kappa x e^{-i\phi} S_2 + x \kappa e^{i\phi} S_2^* - x^2 S_3 + x \kappa S_2 e^{i\phi} - x^2 e^{i\phi} S_3^* + \kappa x S_2^* e^{-i\phi}, \quad (\text{B7})$$

$$f_4 = x e^{-i\phi} (S_3 + S_3^*) - \kappa S_2 - x^2 \kappa S_2^*, \quad (\text{B8})$$

$$f_5 = (S_1 + S_1^*) - x \kappa S_2^* - \kappa x S_2 e^{-i\phi}, \quad (\text{B9})$$

$$f_6 = (S_1 + S_1^*) - \kappa x (e^{i\phi} S_2^* + S_2 e^{-i\phi} + S_2^* e^{-i\phi} + S_2 e^{i\phi}) + x^2 (S_3 + S_3^*), \quad (\text{B10})$$

$$f_7 = x e^{-i\phi} (S_1 + S_1^*) - \kappa x^2 (S_2 + S_2^*) - \kappa x^2 e^{-2i\phi} (S_2 + S_2^*) + x^3 (e^{-i\phi} S_3 + S_3^*), \quad (\text{B11})$$

$$f_8 = -x^2 S_3^* + x \kappa e^{-i\phi} S_2^* - x^2 S_1 + \kappa x^3 S_2 e^{-i\phi}. \quad (\text{B12})$$

Appendix C: Explicit expressions for the resonant coefficients $Im(\chi^{(1,3)}(\delta))$ and $Re(\chi^{(1,3)}(\delta))$

Setting $\omega_{32} = 0$ and $\delta = 0$, the Eqs. (36) and (37) and their corresponding coefficients given in Appendix B simplify, resulting in the following analytical expressions for the linear absorption/dispersion, and third-order (Kerr) nonlinear absorption/dispersion susceptibilities

$$Im(\chi^{(1)}(\delta = 0)) = \frac{N\mu'^2}{\varepsilon_0 \hbar} \frac{\gamma + \gamma' - \kappa x \cos(\phi)}{(\gamma + \gamma')^2 - \kappa^2}, \quad (\text{C1})$$

$$Re(\chi^{(1)}(\delta = 0)) = \frac{N\mu'^2}{\varepsilon_0\hbar} \frac{-\kappa A \sin(\phi)}{(\gamma + \gamma')^2 - \kappa^2}, \quad (C2)$$

$$Im(\chi^{(3)}(\delta = 0)) = \frac{2N\mu'^4}{3\varepsilon_0\hbar^3} \frac{-m_1 \cos(\phi) - m_2 \cos(2\phi) - m_3}{32\gamma'(\gamma + \gamma')((\gamma + \gamma')^2 - \kappa^2)^2}, \quad (C3)$$

$$Re(\chi^{(3)}(\delta = 0)) = \frac{2N\mu'^4}{3\varepsilon_0\hbar^3} \frac{-m_4 \sin(\phi) - m_2 \sin(2\phi)}{32\gamma'(\gamma + \gamma')((\gamma + \gamma')^2 - \kappa^2)^2}, \quad (C4)$$

where

$$m_1 = 4\gamma'x^3\kappa(\gamma + \gamma') - 6x\kappa\gamma(\gamma + \gamma') + 2\gamma x^3\kappa(\gamma + \gamma') - 4\kappa^3x - \kappa^2x^2(\gamma + \gamma') - 7\gamma'\kappa x(\gamma + \gamma') - 4\kappa x\gamma(\gamma + \gamma') - 2x\kappa(\gamma + \gamma')^2 - \kappa x^3(\gamma + \gamma')^2 - \gamma'\kappa x^3(\gamma + \gamma'), \quad (C5)$$

$$m_2 = 2\kappa^2x^2\gamma' + 2\kappa^2x^2(\gamma + \gamma'), \quad (C6)$$

$$m_3 = 2\kappa^2(\gamma + \gamma')(1 + 2x^2) + 2\gamma'\kappa^2(1 - x^2) - 2\gamma'\kappa x(\gamma + \gamma') - \kappa x^3(\gamma + \gamma')^2 + 4\gamma'(\gamma + \gamma')^3(x^2 - 1), \quad (C7)$$

$$m_4 = 3\kappa\gamma'x^3(\gamma + \gamma') + 2\gamma x^3\kappa(\gamma + \gamma') - \kappa^2x^2(\gamma + \gamma') - 5\gamma'x\kappa(\gamma + \gamma') - 2x\kappa(\gamma + \gamma')^2 - \kappa x^3(\gamma + \gamma'). \quad (C8)$$

Appendix D: EM Green's tensor for a 2D periodic nanostructure

The classical EM Green's tensor is defined through the following equation:

$$\nabla \times \nabla \times \mathbf{G}(\mathbf{r}, \mathbf{r}'; \omega) - k^2 \mathbf{G}(\mathbf{r}, \mathbf{r}'; \omega) = \mathbf{1}_3 \cdot \delta(\mathbf{r} - \mathbf{r}'), \quad (D1)$$

where $k = \sqrt{\epsilon_d}\omega/c$ is the wavevector inside the material, ω is the angular frequency of incident light, c is the speed of light in vacuum, and $\mathbf{1}_3$ is the 3×3 unit matrix.

We deal with arrays of macroscopic spheres with 2D periodicity. The method employed here is an EM Green's tensor formalism based on an EM layer-multiple-scattering (LMS) method [67, 68]. The LMS method is ideally suited for the calculation of the transmission/reflection/absorption coefficients of an EM wave incident on slab containing a number of planes of non-overlapping scatterers with the same 2D periodicity. Namely, for each one plane of spheres, the method determines the full multipole expansion of the total multiply scattered wave field and deduces the corresponding transmission and reflection matrices of the whole slab in the plane-wave basis. Having determined the transmission/reflection matrices via the LMS method one can calculate the EM Green's tensor from [10, 69]

$$G_{ii'}^{EE}(\mathbf{r}, \mathbf{r}'; \omega) = g_{ii'}^{EE}(\mathbf{r}, \mathbf{r}'; \omega) - \frac{i}{8\pi^2} \int \int_{SBZ} d^2\mathbf{k}_{\parallel} \sum_{\mathbf{g}} \frac{1}{c^2 K_{\mathbf{g};z}^+} \times v_{\mathbf{g}\mathbf{k}_{\parallel};i}(\mathbf{r}) \exp(-i\mathbf{K}_{\mathbf{g}}^+ \cdot \mathbf{r}) \hat{\mathbf{e}}_{i'}(\mathbf{K}_{\mathbf{g}}^+), \quad (D2)$$

with

$$v_{\mathbf{g}\mathbf{k}_{\parallel};i}(\mathbf{r}) = \sum_{\mathbf{g}'} R_{\mathbf{g}'\mathbf{g}}(\omega, \mathbf{k}_{\parallel}) \exp(-i\mathbf{K}_{\mathbf{g}'}^- \cdot \mathbf{r}) \hat{\mathbf{e}}_i(\mathbf{K}_{\mathbf{g}'}^-), \quad (D3)$$

and

$$\mathbf{K}_{\mathbf{g}}^{\pm} = (\mathbf{k}_{\parallel} + \mathbf{g}, \pm[q^2 - (\mathbf{k}_{\parallel} + \mathbf{g})^2]^{1/2}). \quad (D4)$$

The vectors \mathbf{g} correspond to the reciprocal-lattice vectors associated with the 2D periodic lattice of the plane of scatterers. \mathbf{k}_{\parallel} is the reduced wavevector which lies within the surface Brillouin zone of the corresponding reciprocal lattice [67, 68]. When $q^2 = \omega^2/c^2 < (\mathbf{k}_{\parallel} + \mathbf{g})^2$, $\mathbf{K}_{\mathbf{g}}^{\pm}$ defines an evanescent wave. The term $g_{ii'}^{EE}(\mathbf{r}, \mathbf{r}'; \omega)$ of Eq. (D2) is the free-space Green's tensor and $\hat{\mathbf{e}}_i(\mathbf{K}_{\mathbf{g}}^{\pm})$ denotes the polar unit vector normal to $\mathbf{K}_{\mathbf{g}}^{\pm}$. $R_{\mathbf{g}'; \mathbf{g}}(\omega, \mathbf{k}_{\parallel})$ is the reflection matrix which provides the sum (over \mathbf{g} 's) of reflected beams generated by the incidence of plane wave from the left of the plane of scatterers and is calculated via the LMS method [67, 68]. We note that the above expression [Eqs. (D2)] is derived from the transverse part of the general classical-wave Green's tensor [69]. Also, in Eq. (D2), the terms corresponding to s -polarized waves (those containing components with the azimuthal unit vector $\hat{\mathbf{e}}_i(\mathbf{K}_{\mathbf{g}}^{\pm})$ normal to $\mathbf{K}_{\mathbf{g}}^{\pm}$) have very marginal contribution to the decay rates and have been, justifiably, neglected.

-
- [1] S. M. Sadeghi, *Nanotechnology* 21, 455401 (2010).
- [2] S. G. Kosionis, A. F. Terzis, S. M. Sadeghi, and E. Paspalakis, *J. Phys.: Cond. Matt.* 25, 045304 (2013).
- [3] S. M. Sadeghi, *Phys. Rev. A* 88, 013831 (2013).
- [4] D. Zhao, Y. Gu, J. Wu, J. Zhang, T. Zhang, B. D. Gerardot, and Q. Gong, *Phys. Rev. B* 89, 245433 (2014).
- [5] F. Carreño, M. A. Antón, V. Yannopapas, and E. Paspalakis, *Phys. Rev. B* 95, 195410 (2017).
- [6] S. G. Kosionis and E. Paspalakis, *J. Appl. Phys.* 124, 223104 (2018).
- [7] S. Evangelou, V. Yannopapas, and E. Paspalakis, *Phys. Rev. A* 86, 053811 (2012).
- [8] E. Paspalakis, S. Evangelou, V. Yannopapas, and A. F. Terzis, *Phys. Rev. A* 88, 053832 (2013).
- [9] L. Wang, Y. Gu, H. Chen, J.-Y. Zhang, Y. Cui, B. D. Gerardot, and Q.-H. Gong, *Scient. Rep.* 3, 2879 (2013).
- [10] V. Yannopapas, E. Paspalakis, and N. V. Vitanov, *Phys. Rev. Lett.* 103, 063602 (2009).
- [11] S. Evangelou, V. Yannopapas, and E. Paspalakis, *Phys. Rev. A* 83, 055805 (2011).
- [12] S. Evangelou, V. Yannopapas, and E. Paspalakis, *Phys. Rev. A* 83, 023819 (2011).
- [13] Y. Gu, L. Wang, P. Ren, J.-X. Zhang, T.-C. Zhang, J.-P. Xu, S.-Y. Zhu, and Q.-H. Gong, *Plasmonics* 7, 33 (2012).
- [14] Y. Gu, L. Wang, P. Ren, J.-X. Zhang, T.-C. Zhang, O. J. F. Martin, and Q.-H. Gong, *Nano Lett.* 12, 2488 (2012).
- [15] W. Zhang, A. O. Govorov, and G. W. Bryant, *Phys. Rev. Lett.* 97, 146804 (2006).
- [16] R. D. Artuso and G. W. Bryant, *Phys. Rev. B* 82, 195419 (2010).
- [17] M. R. Singh, D. G. Schindel, and A. Hatef, *Appl. Phys. Lett.* 99, 181106 (2011).
- [18] S. G. Kosionis, A. F. Terzis, V. Yannopapas, and E. Paspalakis, *J. Phys. Chem. C* 116, 23663 (2012).
- [19] A. V. Malyshev and V. A. Malyshev, *Phys. Rev. B* 84, 035314 (2011).
- [20] B. S. Nugroho, V. A. Malyshev, and J. Knoester, *Phys. Rev. B* 92, 165432 (2015).
- [21] F. Carreño, M. A. Antón, and E. Paspalakis, *J. Appl. Phys.* 124, 113107 (2018).
- [22] M. R. Singh, *Nanotechnology* 24, 125701 (2013).
- [23] J.-B. Li, N.-C. Kim, M.-T. Cheng, L. Zhou, Z.-H. Hao, and Q.-Q. Wang, *Opt. Express* 20, 1856 (2012).
- [24] E. Paspalakis, S. Evangelou, S. G. Kosionis, and A. F. Terzis, *J. Appl. Phys.* 115, 083106 (2014).
- [25] S. K. Singh, M. K. Abak, and M. E. Tasgin, *Phys. Rev. B* 93, 035410 (2016).
- [26] H. Schmidt and A. Imamoglu, *Opt. Lett.* 21, 1936 (1996).
- [27] H. Wang, D. Goorskey, and M. Xiao, *Phys. Rev. Lett.* 87, 073601 (2001).
- [28] Y.-P. Niu and S.-Q. Gong, *Phys. Rev. A* 73, 053811 (2006).
- [29] H. R. Hamed and G. Juzeliuñas, *Phys. Rev. A* 91, 053823 (2015).
- [30] A. Imamoglu, H. Schmidt, G. Woods, and M. Deutsch, *Phys. Rev. Lett.* 79, 1467 (1997).
- [31] M. M. Kash, V. A. Sautenkov, A. S. Zibrov, L. Hollberg, G. R. Welch, M. D. Lukin, Y. Rostovtsev, E. S. Fry, and M. O. Scully, *Phys. Rev. Lett.* 82, 5229 (1999).
- [32] S. Evangelou, V. Yannopapas, and E. Paspalakis, *J. Mod. Opt.* 61, 1458 (2014).
- [33] H. Chen, J. Ren, Y. Gu, D.-X. Zhao, J. Zhang, and Q. Gong, *Sci. Rep.* 5, 18315 (2015).
- [34] A. F. Terzis, S. G. Kosionis, J. Boviatsis, and E. Paspalakis, *J. Mod. Opt.* 63, 451 (2016).
- [35] J. Ren, H. Chen, Y. Gu, D.-X. Zhao, H. Zhou, J. Zhang, and Q. Gong, *Nanotechnology* 27, 425205 (2016).
- [36] M. M. Tohari, A. Lyras, and M. S. AlSalhi, *Nanomaterials* 8, 521 (2018).
- [37] S. G. Kosionis and E. Paspalakis, *J. Phys. Chem. C* 123, 7308 (2019).
- [38] A. Vaziri, J.-W. Pan, T. Jennewein, G. Weihs, and A. Zeilinger, *Phys. Rev. Lett.* 91, 227902 (2003).
- [39] M. Woerdemann, C. Alpmann, M. Essling, and C. Denz, *Laser Photon. Rev.* 7, 839 (2013).
- [40] D. J. Stevenson, F. G. Moore, and K. Dholakia, *J. Biomed. Opt.* 15, 041503 (2010).
- [41] M. P. Macdonald, L. Paterson, K. V. Sepulveda, J. Arlt, W. Sibbett, and K. Dholakia, *Science* 296, 1101 (2002).
- [42] V. E. Lembessis and M. Babiker, *Phys. Rev. A* 82, 051402 (2010).
- [43] V. E. Lembessis, D. Ellinas, M. Babiker, and O. Al-Dossary, *Phys. Rev. A* 89, 053616 (2014).
- [44] Q.-F. Chen, B.-S. Shi, Y.-S. Zhang, and G.-C. Guo, *Phys. Rev. A* 78, 053810 (2008).
- [45] G. Walker, A. S. Arnold, and S. Franke-Arnold, *Phys. Rev. Lett.* 108, 243601 (2012).
- [46] D.-S. Ding, Z.-Y. Zhou, B.-S. Shi, X.-B. Zou, and G.-C. Guo, *Opt. Lett.* 37, 3270 (2012).
- [47] L. Han, M. Cao, R. Liu, H. Liu, W. Guo, D. Wei, S. Gao, P. Zhang, H. Gao, and F. Li, *Europhys. Lett.* 99, 34003 (2012).
- [48] N. Radwell, T. W. Clark, B. Piccirillo, S. M. Barnett, and S. Franke-Arnold, *Phys. Rev. Lett.* 114, 123603 (2015).

- [49] S. Sharma and T. N. Dey, *Phys. Rev. A* 96, 033811 (2017).
- [50] H. R. Hamed, V. Kudriasov, J. Ruseckas, and G. Juzeliunas, *Opt. Express* 26, 28249 (2018).
- [51] J. Ruseckas, G. Juzeliūnas, P. Öhberg, and S. M. Barnett, *Phys. Rev. A* 76, 053822 (2007).
- [52] H. R. Hamed, J. Ruseckas, and G. Juzeliūnas, *Phys. Rev. A* 98, 013840 (2018).
- [53] J. Ruseckas, A. Mekys, and G. Juzeliūnas, *Phys. Rev. A* 83, 023812 (2011).
- [54] Z. Dutton and J. Ruostekoski, *Phys. Rev. Lett.* 93, 193602 (2004).
- [55] J. Ruseckas, V. c. v. Kudriasov, I. A. Yu, and G. Juzeliūnas, *Phys. Rev. A* 87, 053840 (2013).
- [56] H. R. Hamed, J. Ruseckas, E. Paspalakis, and G. Juzeliūnas, *Phys. Rev. A* 99, 033812 (2019).
- [57] D. Moretti, D. Felinto, and J. W. R. Tabosa, *Phys. Rev. A* 79, 023825 (2009).
- [58] D. Bortman-Arbiv, A. D. Wilson-Gordon, and H. Friedmann, *Phys. Rev. A* 63, 031801 (2001).
- [59] H. R. Hamed, E. Paspalakis, G. Zlabys, G. Juzeliūnas, and J. Ruseckas, *Phys. Rev. A* 100, 023811 (2019).
- [60] G. S. Agarwal, *Phys. Rev. Lett.* 84, 5500 (2000).
- [61] M. Kiffner, M. Macovei, J. Evers, and C. H. Keitel, *Prog. Opt.* 55, 85 (2010).
- [62] Y. Yang, J. Xu, H. Chen, and S. Zhu, *Phys. Rev. Lett.* 100, 043601 (2008).
- [63] G.-X. Li, J. Evers, and C. H. Keitel, *Phys. Rev. B* 80, 045102 (2009).
- [64] P. K. Jha, X. Ni, C. Wu, Y. Wang, and X. Zhang, *Phys. Rev. Lett.* 115, 025501 (2015).
- [65] S. Hughes and G. S. Agarwal, *Phys. Rev. Lett.* 118, 063601 (2017).
- [66] V. Karanikolas and E. Paspalakis, *J. Phys. Chem. C* 122, 14788 (2018).
- [67] N. Stefanou, V. Yannopoulos, and A. Modinos, *Comp. Phys. Commun.* 113, 49 (1998).
- [68] N. Stefanou, V. Yannopoulos, and A. Modinos, *Comp. Phys. Commun.* 132, 189 (2000).
- [69] R. Sainidou, N. Stefanou, and A. Modinos, *Phys. Rev. B* 69, 064301 (2004).
- [70] D. Bortman-Arbiv, A. D. Wilson-Gordon, and H. Friedmann, *Phys. Rev. A* 63, 043818 (2001).
- [71] L. Allen, M. J. Padgett, and M. Babiker, *Progress in Optics* 39, 291 (1999).